Limits of the macrospin model in cobalt nanodots with enhanced edge magnetic anisotropy

S. Rohart,[1,2,3,*] V. Repain,[1] A. Thiaville,[2] and S. Rousset[1]

[1]*Laboratoire Matériaux et Phénomènes Quantiques, CNRS, Université Paris 7, UMR 7162, 2 Place Jussieu, F-75251 Paris, France*

[2]*Laboratoire de Physique des Solides, CNRS, Université Paris Sud, UMR 8502, Bâtiment 510, F-91405 Orsay Cedex, France*

[3]*Laboratoire de Physique de la Matière Condensée et Nanostructures, CNRS, Université Lyon 1, UMR 5586, Domaine Scientifique de la Doua, F-69622 Villeurbanne Cedex, France*

(Received 22 December 2006; revised manuscript received 30 May 2007; published 5 September 2007)

We report on a theoretical study, by an atomic scale micromagnetic model, of the magnetic configurations and magnetization reversal in cobalt circular nanodots (one and two atomic layers thick, up to 10 nm in diameter) with enhanced magnetocrystalline anisotropy at the edge. According to the dot diameter, out-of-plane, twisted, and in-plane configurations are found. The results are first compared to the macrospin model, usually applied to this type of nanoparticles, and then to a continuous micromagnetic model with a sole radial variation of the magnetization. Field induced magnetization switching is also computed. We observe a process close to coherent rotation for nanodot diameters as small as 2 nm, but with a lower switching field as compared to the macrospin model, that may be called quasiuniform rotation. Our results fix the application limits of the macrospin model, which forgets atomic-scale variation of the properties.

DOI: 10.1103/PhysRevB.76.104401 PACS number(s): 75.75.+a, 75.40.Mg

I. INTRODUCTION

Magnetic clusters, with dimensions in the nanometer range, are driving a considerable interest due to their potential application in ultrahigh density data storage. At this size, the exchange energy dominates the demagnetizing energy (dipolar coupling) in the energy balance. As exchange energy tends to align neighboring spins, the complex micromagnetic structure is generally simplified to the macrospin model:[1] the magnetic configuration is thought to be monodomain and the magnetization reversal to be coherent (i.e., all the spins are always parallel to each other during the magnetization reversal). This assumption leads to simple models first described by Stoner and Wohlfarth,[2] which give insights about the static and dynamic behaviors of the magnetization in nanostructures.[2–8] The simplicity of these models makes them very appealing, and most experiments are indeed discussed through them.[5,6,9–14] However, the phenomena at this scale are richer than this simplicity. For example, ferrimagnetic oxide clusters such as γ-Fe_2O_3 have shown a surface spin disorder due the breaking of the symmetry at the surface that induces some important deviation to the macrospin model, like an absence of magnetization saturation at low temperature in high magnetic fields.[15] In metallic clusters, the increase of the surface magnetic anisotropy recently reported[11,14,16] also drives the need to consider the limits of the macrospin model and establish new models. Indeed, as the exchange energy, when considered as a first neighbor interaction, is decreased at the surface due to the low coordination, the enhanced magnetic anisotropy at the surface may cause different behaviors for the surface and volume spins. On the theoretical point of view, this problem has already been addressed in the case of clusters with a radial magnetic anisotropy.[17–20] These studies have shown that for a ratio between atomic surface anisotropy and exchange energies higher than 1, the magnetization reversal is not coherent and surface spins switch independently of the volume spins.

Among the more recent experimental results, cobalt nanodots grown on Pt(111) (Ref. 14) and Au(111) [Refs. 21 and 22] have given impressive examples of enhanced magnetic anisotropy at the lower coordinated atoms. In these two dimensional structures, the experiments have shown that the magnetic anisotropy is mainly distributed at the edge atoms, which induce an easy magnetization axis perpendicular to the surface. Without this contribution, the nanodots would be magnetized in plane. However, in these two studies, this determination relied on macroscopic magnetometry measurements and on their analysis using the macrospin model. A recent study of Co/Pt(111) nanodots using spin resolved scanning tunneling microscopy[23] has contested this interpretation, claiming that the magnetic anisotropy in the center of the dots is perpendicular. This poses the question of the validity of the model used to analyze these first experiments. Following the model of Ref. 14 with the enhanced anisotropy at the edge spins, the hypothesis of homogeneous magnetization is not trivial as the edge and center spins have different easy magnetization axes (perpendicular or in plane). In this study, we use this enhanced edge anisotropy model and perform a micromagnetic study at the atomic level and at zero temperature, in order to determine the magnetic configurations in the dots. For mono- and bilayer thick dots with diameter up to 10 nm, corresponding to the experimental case of Refs. 14 and 21, we study the magnetic configurations and the field induced magnetization reversal and compare these results to the macrospin model. A continuous micromagnetic model is also introduced in order to obtain a phase diagram of the magnetic configuration versus the parameters.

II. ATOMIC MODEL

The aim of the calculation is to obtain the minimum energy magnetic configurations in ferromagnetic nanodots and at zero temperature. The magnetic energy is written as

$$E = -\mu_0\mu\mathbf{H}\sum_i \mathbf{m}_i - J\sum_{\langle i,j\rangle} \mathbf{m}_i\cdot\mathbf{m}_j - \sum_i k_i(\mathbf{m}_i\cdot\mathbf{e}_i)^2 - \frac{\mu_0\mu^2}{8\pi}\sum_{i,j\neq i}\left[\frac{3(\mathbf{m}_i\cdot\mathbf{r}_{ij})(\mathbf{m}_j\cdot\mathbf{r}_{ij})}{r_{ij}^5} - \frac{\mathbf{m}_i\mathbf{m}_j}{r_{ij}^3}\right], \quad (1)$$

where $\mathbf{m}_i$ is the atomic magnetic moment unit vector on site i, μ the atomic magnetic moment, and $\mathbf{r}_{ij}$ is the vector connecting sites i and j. The sum contains four terms: (i) the Zeeman energy, (ii) the exchange coupling between first neighbors (with J the exchange energy per bond), (iii) the magnetocrystalline anisotropy energy (MCA, expressed as a second degree local anisotropy with k_i the anisotropy energy and $\mathbf{e}_i$ the anisotropy axis on site i), and (iv) the dipolar coupling between magnetic moments. Note that this description assumes classical localized magnetic moments. The magnetization configuration which minimizes Eq. (1) is calculated by integrating, from a nonequilibrium state, the Landau-Lifchitz-Gilbert (LLG) equation

$$\frac{d\mathbf{m}_i}{dt} = \gamma_0\mathbf{H}_i^{\text{eff}}\times\mathbf{m}_i + \alpha\mathbf{m}_i\times\frac{d\mathbf{m}_i}{dt}, \quad (2)$$

where γ_0 is the gyromagnetic ratio ($\gamma_0>0$) and α is the damping factor (taken as 0.5 in order to ensure a fast integration convergence). The effective field $\mathbf{H}_i^{\text{eff}}$ acting on the magnetic moment $\mathbf{m}_i$ describes the influence of the anisotropy and the other magnetic moments as

$$\mathbf{H}_i^{\text{eff}} = -\frac{1}{\mu_0\mu}\frac{\partial E}{\partial\mathbf{m}_i}. \quad (3)$$

For a particle containing N magnetic moments, we obtain a set of $3N$ coupled equations. The LLG equation is numerically integrated with a time step of 1 fs which was found to be a good compromise between accuracy and calculation speed. The minimum energy configuration is found by relaxing the LLG equation until $|d\mathbf{m}_i/dt|<10^{-6}$ rad/fs.

We focus on mono- and bilayer thick circular Co nanodots with diameters up to 10 nm. The cylindrical axis is called the z axis. The atoms have a hexagonal stacking with a lattice parameter $a=2.5$ Å. The atomic magnetic moment is $\mu=2.1\mu_B$ ($M_S=1.77\times10^6$ A/m).[14,22] The exchange energy is taken as $J=8.4$ meV per bond [for a three-dimensional (3D) material, it corresponds to an exchange constant $A_{3D}=0.75\times10^{-11}$ J/m (Ref. 24)]. Following the experimental results on Co nanoparticles on Au(788) and Pt(111), we are interested in perpendicular MCA and take $\mathbf{e}_i=\mathbf{e}_z\,\forall\, i$. We consider the extreme case proposed in Ref. 14, where MCA is only due to the edge atoms ($k_i=0$ for the atom i in the center, $k_i=k$ for the atom i at the edge). We take $k=0.6$ meV, close to the experimental values.[14,21] For comparison, we also consider the case with a homogeneous MCA, with $k_i=k'\,\forall\, i$. For a given size, we adjust k' so that the total MCA is the same in both cases. It is worth noticing that in the macrospin approximation, the dipolar interaction induces an effective shape magnetic anisotropy (SMA), with z as the hard axis, as the diameter is higher than the thickness (we denote by $\mathcal{K}_d$ the increase of SMA energy from uniform in-plane to perpendicular states). This energy is exactly evaluated by summing the dipole-dipole interactions over the whole dot.[25] In terms of characteristic length scales, the usual 3D exchange length $\Lambda=\sqrt{2A_{3D}/\mu_0M_S^2}$ is 2 nm here and a bulk material with a homogeneous MCA of 0.6 meV/at. ($K=8.7\times10^6$ J/m^3) has a Bloch wall width $\delta=\sqrt{A_{3D}/K}$ of 2 nm.

III. ZERO FIELD MAGNETIC CONFIGURATIONS

We first address results on the magnetic configurations at equilibrium under zero field. On the micromagnetic point of view, the magnetic configurations are determined by the competition, at a local scale, of the three different energies: exchange, magnetocrystalline anisotropy, and dipolar coupling. Unlike the first two that are local, the dipolar energy is long ranged. With increasing the dot size, its strength increases, which leads to a variety of configurations versus the dot diameter. Moreover, at the edge spins, the MCA and dipolar coupling energies have opposite tendencies: the MCA tends to align the spins along the z axis, whereas the dipolar coupling tends to align them along the longest direction of the structure, i.e., perpendicular to the z axis. In the macrospin picture, the situation is simpler as the exchange energy is supposed to be infinite. In that case, local quantities can be avoided and only the integral energies have to be considered. The total MCA is proportional to the number of edge atoms (approximately proportional to $\sqrt{N}$). Neglecting in a first approximation the dot diameter variation of the thickness to diameter ratio, the SMA is proportional to the number of atoms N (a more accurate model including the aspect ratio is discussed below). Thus, MCA dominates at lower size, whereas SMA dominates at higher size and the magnetization direction is expected to switch from perpendicular to in-plane direction above a critical size. Once more, as both MCA and SMA are second degree in $\mathbf{m}$, the transition is expected to be abrupt with no intermediate tilted states.

Using the parameters given above for Co, the critical diameters are expected to be 5.75 and 6.15 nm, respectively, for mono- and bilayer dots (note that the higher critical diameter for bilayer dots is due to a lower demagnetizing factor, linked to the thickness to diameter ratio[26]). The variation of the angle θ between the total moment and the z axis is shown in Fig. 1(a), as computed for mono- and bilayer dots. As expected in the macrospin model, a reorientation transition is clearly evidenced. For both thicknesses, the moments lie along the z axis for diameters lower than 5 nm and in the (x,y) plane for diameters higher than 9 nm. However, the transition appears to be smooth and tilted magnetization states are found. These tilted magnetization states are inhomogeneous as the magnetic moments at the edge are less tilted than the magnetic moments at the dot center, due to the edge MCA [see the example of a 5.25 nm diameter monolayer particle in Figs. 1(b) and 1(c)]. This result is in contradiction with the macrospin model. Note that, on the contrary, we have found that when MCA is homogeneously distributed over the whole particle, the magnetic configurations are always homogeneous and no twisted states are found.

This result is, in fact, analogous to the twisted spin configurations predicted in magnetic multilayers with perpen-

dicular interface magnetic anisotropy.[27,28] In that case, the authors predicted twisted spin configurations when the total MCA and SMA nearly compensate. In our case, the edge MCA is analogous to the thin film interface magnetic anisotropy. We generalize here the model from Ref. 27 to our cylindrical geometry. The magnetic configuration is described in a continuous approximation by $\theta(r)$, the angle between the magnetic moment at position r with the z direction, where r is the distance from the particle center. Note that (i) all moments are assumed to tilt toward the same in-plane direction and (ii) a cylindrical symmetry is assumed for this function, with no dependence on thickness as it is only a few atomic layers. These assumptions come from the structures obtained with the atomic model, as shown in Fig. 1. For a cylindrical dot, with thickness t and radius R, the magnetic energy E is

$$\frac{E[\theta(r)]}{2\pi t} = \int_0^R \left[A\left(\frac{d\theta}{dr}\right)^2 + K_d \cos^2\theta \right] r dr + RK_e \sin^2\theta. \tag{4}$$

The first term in the integral is the exchange energy, with $A=\lambda J\sqrt{2}/a$ (where $\lambda=\frac{3}{4}$ and $\frac{7}{8}$, respectively, for the mono- and bilayer dots). The second one is the SMA, with $K_d = X\eta(R/t)\mu_0 M_S^2/2$ [where $M_S=\sqrt{2}\mu/a^3$ is the magnetization; $X=0.932$ and 0.966 for the mono- and bilayer dots, respectively, account for the discrete lattice effect[25] and $\eta(R/t)$ accounts for the dot cylindrical shape[26]]. It is assumed for simplicity that SMA is homogeneous over the whole particle and thus one has, in terms of the uniform demagnetizing factors, $\eta=N_z-N_x$. The last term is the edge MCA with $K_e = k\sqrt{3/2}/a^2$. The function $\theta(r)$ which minimizes the energy is the solution of the following equation obtained by variational calculus

$$u\frac{d^2\theta}{du^2} + \frac{d\theta}{du} + u\sin\theta\cos\theta = 0 \quad \text{for } 0 \leqslant u \leqslant R/\Lambda, \tag{5a}$$

$$\frac{d\theta}{du} = -\rho\sin\theta\cos\theta \quad \text{for } u = R/\Lambda \equiv u_{\max}, \tag{5b}$$

where $u=r/\Lambda$, $\Lambda=\sqrt{A/K_d}$ is the usual exchange length, and $\rho=K_e/\sqrt{AK_d}$ is a nondimensional parameter proportional to the edge anisotropy. Although the case of the infinite thin film has an analytical solution,[27] it does not in our geometry. Therefore, Eqs. (5a) and (5b) are solved numerically by the shooting method (an initial value $\theta(0)$ results in a given profile of θ at $u=u_{\max}$ that is compared to the boundary condition [Eq. (5b)]). A general phase diagram versus the two parameters $R/2\Lambda$ and ρ can be constructed and is shown in Fig. 2. Its shape is very similar to that obtained analytically in the case of an ultrathin film.[27]

Profiles of the magnetization inside the nonuniform region are shown in Fig. 3, evidencing that nonuniformity decreases at the phase boundaries. In order to compare these results with those of the atomic model, the dependence of the demagnetizing factors on the aspect ratio cannot be neglected. In addition, as the atomic disks are not perfectly circular, it is necessary to multiply K_d and K_e by factors F_d and F_e so that the same number of total and perimeter atoms is considered (we found $F_d=0.95$ and $F_e=1.1$). The calculated continuous micromagnetic curves obtained under these conditions have been superposed to the atomic model results in Figs. 1(a) and 1(b), showing a good agreement. The differences that remain between the two model are small once the proper effective micromagnetic parameters are used.

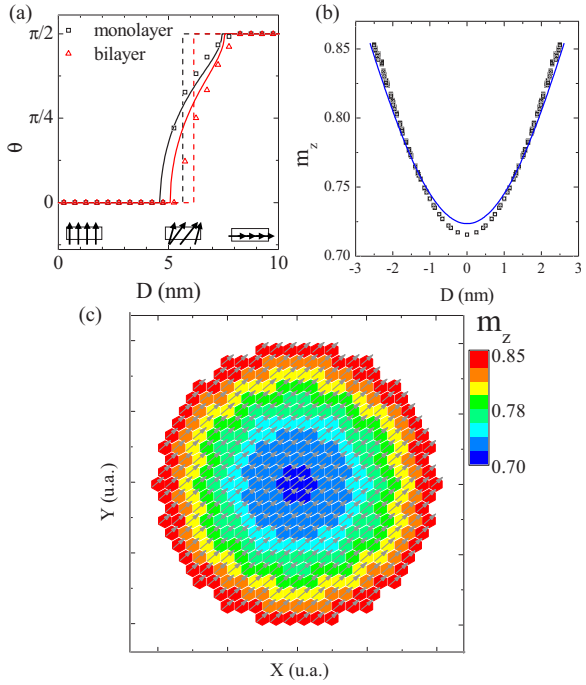

FIG. 1. (Color online) (a) Variation of the angle θ between the total moment and the z axis (cylindrical axis) versus the dot diameter, for monolayer (black squares) and bilayer (gray triangles) nanodots. Both calculations [in black (gray) for monolayer (bilayer) dots] are compared to the macrospin model (dashed lines) and the continuous micromagnetic model (continuous lines) described in the text. The sketches indicate the typical calculated magnetic configuration: out of plane, twisted, and in plane. [(b) and (c)] Twisted magnetic configuration for a 5.25 nm diameter monolayer dot. Panel (b) corresponds to the magnetization profile as a function of the distance from the particle center (the points correspond to all atomic positions in the atomic calculation and the line to the continuous micromagnetic model). Picture (c) is a magnetization map [the arrows indicate the magnetic moment projection in the (x,y) plane and the gray points indicate the magnetic moment projection on the z axis].

The discrete character in the atomic model, not included in the continuous model, does not have a dramatic impact on the results, the edge roughness being only taken into account via the renormalization of the demagnetizing and edge anisotropy energies. Moreover, the attenuated exchange and nonuniform demagnetizing energy terms at the edges, not included in the continuous model, are not essential features to reproduce the results. Thus, we see that using physically reasonable atomic parameters, although the macrospin model is clearly inadequate, the essential features of the magnetization states can be obtained through continuous micromagnetics. In particular, no decoupling of edge from bulk is observed

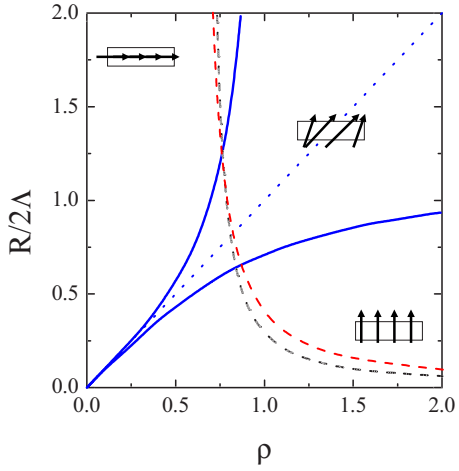

FIG. 2. (Color online) The three possible magnetization states, two uniform and one nonuniform (indicated by the sketches), in a circular disk of radius R, as a function of the two nondimensional parameters ρ and $R/2\Lambda$. The continuous blue curves correspond to the phase diagram of the continuous micromagnetic calculation and delimit the three possible states. The dotted straight line with $R/2\Lambda=\rho$ corresponds to the macrospin phase diagram, where no twisted states are predicted: the magnetization is either parallel ($R/2\Lambda<\rho$) or perpendicular to the z axis ($R/2\Lambda>\rho$). The dashed black (red) curve indicates the change of effective parameters for monolayer (bilayer) dots. Note that these curves are not simple straight lines with ρ=const because they include the fact that the demagnetizing factor (and thus the exchange length) varies with the dot size.

here, contrary to more extreme cases investigated previously.[17,18]

IV. FIELD-INDUCED MAGNETIZATION REVERSAL

We now consider the magnetization reversal induced by an external magnetic field. Using the atomic simulation, the dot hysteresis loops are calculated in a quasistatic mode by increasing the external field strength step by step and relaxing the magnetic configuration using the LLG equation after each increment. The magnetization switching field H_C corresponds to the critical field above which the magnetization jumps irreversibly from an energy minimum to an other one. Calculations were also performed in the continuous micromagnetic model. Instead of the differential equation [Eq. (5a)], a slightly different equation has to be solved in the presence of an applied field,

$$u\frac{d^2\theta}{du^2}+\frac{d\theta}{du}+u\sin\theta\cos\theta-uh\sin(\theta-\gamma)=0, \qquad (6)$$

where γ is the angle at which the field is applied with respect to the z axis and $h=H/[MX\eta(R/t)]$ is the reduced field modulus. Starting from $\mu_0H=1$ T, the field was decreased up to -1 T by steps $\mu_0\Delta H=1$ mT. For each field, a $\theta(u)$ profile was found as discussed previously. Reversal was detected by an abrupt change of the solution.

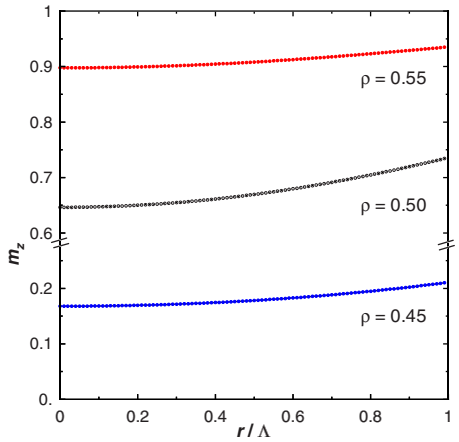

FIG. 3. (Color online) Profiles of the magnetization (perpendicular magnetization component m_z) versus radial position r, for a disk with radius $R=\Lambda$ and three values of the parameter ρ.

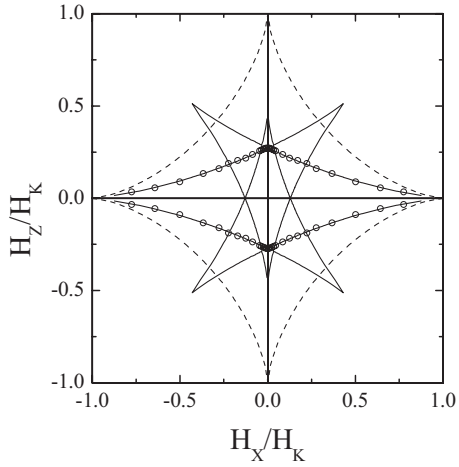

FIG. 4. Switching field astroids for the 5.25 nm diameter monolayer dots. The magnetic fields are normalized to the anisotropy field ($\mu_0H_K=0.55$ T). The dots correspond to the atomic simulation, the continuous line to the continuous micromagnetic calculation, and the dashed line to coherent magnetization reversal.

The magnetization switching field has been calculated as a function of the angle γ in order to obtain the so-called astroid curve. The results are first compared with the macrospin model, i.e., for a coherent rotation (CR) of the spins. Again, this model provides a very simple description of the switching field, which only involves average quantities. When $\gamma=0$, it predicts that the switching field (H_C^{CR}) equals the anisotropy field H_K,

$$H_C^{\mathrm{CR}}(\gamma=0)=H_K=\frac{2k_{\mathrm{eff}}}{\mu_0\mu}, \qquad (7)$$

where $k_{\mathrm{eff}}=(\Sigma_i k_i-\mathcal{K}_d)/N$ is the mean anisotropy energy per atom. When $\gamma\neq0$, $H_C^{\mathrm{CR}}(\gamma)$ is exactly calculated from the Stoner-Wohlfarth solution.[29]

The simulations with the nanodots which are magnetized in the twisted magnetic configuration show a strong disagreement with the CR astroid (see one example in Fig. 4). Indeed, we observe a strong reduction of the switching field as compared to the CR switching field, particularly for an

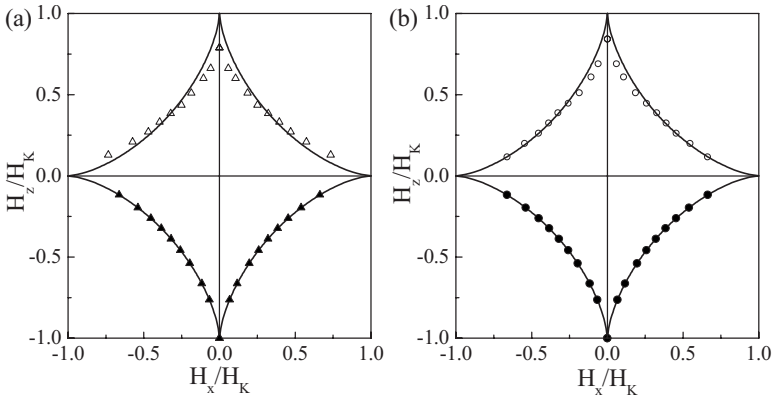

FIG. 5. Switching field astroids for 3.25 nm diameter (a) monolayer and (b) bilayer dots. The upper parts (open points) correspond to the edge MCA cases and the lower parts (full points) correspond to the homogeneous MCA case. The lines correspond to the macrospin switching field astroid. The value of the anisotropy field is $\mu_0 H_K = 1.46$ and 1.72 T for, respectively, mono- and bilayer dots.

external field aligned along the z axis. This is understood easily by considering the torque applied by the external field on the magnetization: in the macrospin model, the magnetization is parallel to the external field and the torque is small; in the twisted state, the magnetization is tilted and the torque is stronger.

The micromagnetic model displays an even more complex curve, which fits the simulation results but also shows additional tips in tilted directions. These tips are due to the lower degree of freedom in the micromagnetic model (two dimensional moments) than in the atomic simulation (3D moments), and the disappearance of such tips under rotation symmetry has been discussed elsewhere.[8] The deformed astroid and particularly the presence of many tips in it are generally seen as the signature of higher order anisotropy terms.[8,29] In our case, this interpretation is not suitable as all anisotropies are second degree in **m**. It is, in fact, related to a noncoherent magnetization reversal. Due to the different magnetization configurations, the energy variation versus the mean magnetization direction is not simply due to the magnetocrystalline and shape anisotropies but also includes an effective configuration anisotropy. The first order deviation to the macrospin is seen as an effective configuration energy with a cubic (fourth order) symmetry,[19] which can be evidenced in the astroid.[29,30] We evaluate this effective configuration anisotropy in the example of the 5.25 nm monolayer dot shown in Fig. 4. Considering the magnetocrystalline and shape anisotropies, the magnetic anisotropy energy has a uniaxial form

$$E_a = k_{\text{eff}} \sin^2 \theta, \tag{8}$$

with $k_{\text{eff}} = 8.7$ μeV/at. To fit the astroid in Fig. 4 in the framework of the coherent magnetization reversal,[29] we use the effective anisotropy energy,

$$E_a^{\text{eff}}(\theta) = k_1 \sin^2 \theta \cos^2 \theta + k_u \sin^2 \theta. \tag{9}$$

We have found $k_1 = 24$ μeV/at. and $k_u = 6$ μeV/at. (note that the fit can be further improved using even higher order terms but that the essential correction to the CR is the fourth order one). The uniaxial anisotropy constant k_u is close to k_{eff}. Thus, most of the deviation to the macrospin is found in the fourth order anisotropy constant K_1, which represents the configuration anisotropy, in good qualitative agreement with Ref. 19.

By considering the torque acted by the field on the magnetization, the deviation from the CR model is not surprising for the particles that display a twisted configuration. However, we have also identified some important deviations for the particles with diameter well below 5 nm, as shown in Fig. 5. Due to the edge MCA (Fig. 5, upper parts), the macrospin model only approximately reproduces the calculation and a slight deviation is observed. This is particularly evident when the field direction is close to the anisotropy axis ($|\gamma| < 20°$), where the switching field is found to be lower than the coherent magnetization switching field. Note that in the case of a uniform MCA distribution (Fig. 5, lower parts), the agreement between the macrospin model and the calculation is quite perfect. In the case of the edge anisotropy, the moments at the center of the dot tend to reverse earlier than those of the edge atoms. They further induce the switching of the edge moments via the exchange coupling.

Focusing on the case with a field aligned along the z axis, we further compare the simulation results with the macrospin model, as detailed in Fig. 6. In the macrospin model, the switching field is given by Eq. (7) and approximately decreases with dot diameter linearly with $N^{-1/2}$. The simulation for diameters below the critical diameter approximately fol-

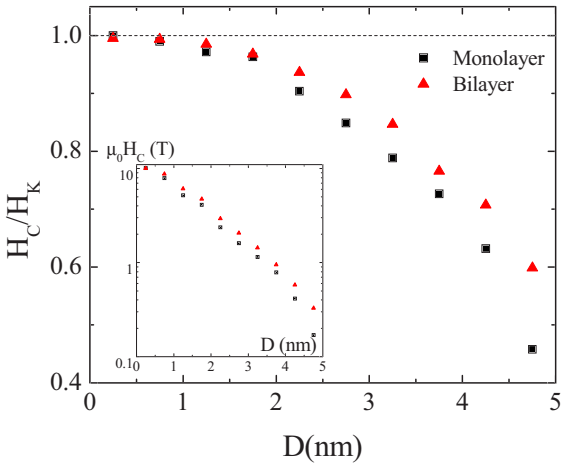

FIG. 6. (Color online) Atomic simulation of the switching field (H_C) versus the dot size, for H aligned along the z axis. In the main figure, H_C is normalized to the coherent rotation switching field. The inset displays the absolute value of H_C.

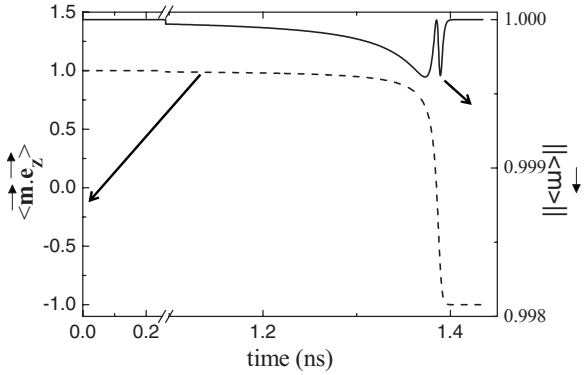

FIG. 7. Time trace of the magnetization reversal in a 2.25 nm bilayer dot. A magnetic field ($\mu_0 H$=2.1 T) is applied at t=0 s along the z axis and is opposite to the initial moment direction. Dashed line: projection of the total moment along the z axis. Full line: norm of the total moment. Note that the absolute value of the time is irrelevant as the damping α in the simulation is high as compared to the reality. Using α=0.1 as a more realistic value, the switching time is about 6.9 ns (1.4 ns in the present result with α=0.5). However, the reversal mode is not specific to this overdamped calculation.

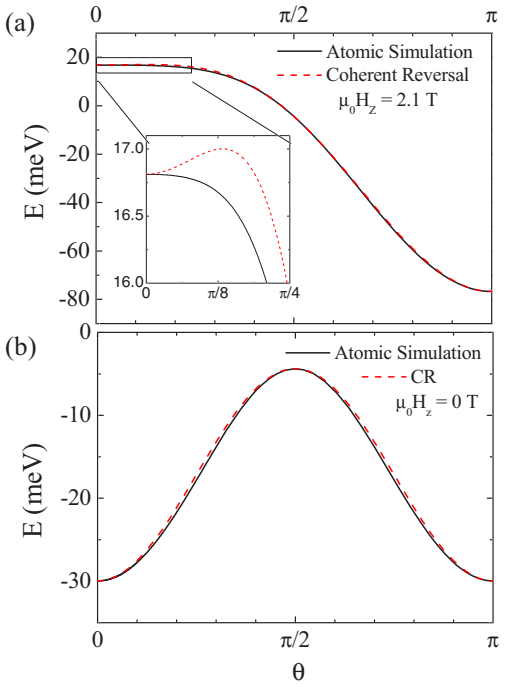

FIG. 8. (Color online) Energy versus the angle θ between the total moment and the z axis for a 2.25 nm bilayer dot, for (a) $\mu_0 H$=2.1 T (H/H_K=0.84) and (b) H=0, in the case of a coherent (macrospin model) and a quasiuniform (atomic simulation) rotation of the magnetization The inset is a zoom close to the origin.

lows this trend but, as already noticed from the astroids, the macrospin model tends to overestimate the switching field. As soon as the diameter is higher than 1 nm, a deviation is clearly evidenced. This deviation increases with the dot diameter and is more than 40% for a 4.75 nm diameter bilayer dot (50% for a monolayer dot). Note that the deviation is mainly due to the inhomogeneous MCA distribution, although dipolar coupling also plays some role. Indeed, we have calculated the switching field without taking into account the dipolar effects and found that the difference between the calculation and macrospin model is about 15% for the 4.75 nm diameter bilayer dot.

The noncoherent magnetization reversal in the dots is clearly evidenced in Fig. 7, where the norm of the total moment is shown to vary during the magnetization reversal. The dot magnetic moments are not perfectly parallel to each other and a maximum angle of 2° opens between the edge and center moments. This indicates that the reversal occurs via nonuniform magnetic states similar to the twisted magnetic configurations found previously for the dots with higher diameters. However, although the norm of the total moment varies by less than 0.05%, the change of the switching field is non-negligible. So, this type of reversal may be called *quasiuniform rotation*.[5] In this case, the reversal is initiated at the center moments, which have a zero MCA, and is further induced to the edge moments via the exchange coupling.

Up to now, we have discussed the nanodot switching at T=0 K. An important question concerns what happens at finite temperature. Indeed, magnetization reversal in such particles is known to be thermally activated. The energy barrier for switching (i.e., the difference between the maximum and initial energies during magnetization reversal) is the key parameter which determines the transition to the superparamagnetic regime[14,21,22] via the Néel-Brown law. In the case of dots with an edge MCA, we have calculated the energy variation versus the magnetization direction for a coherent and a quasiuniform magnetization rotation (see Fig. 8 for the same 2.25 nm diameter bilayer dot presented in Fig. 7). When a magnetic field which lies between the quasiuniform switching field H_C and the coherent switching field H_C^{CR} is applied, the coherent rotation still displays an energy barrier ΔE to switch from the initial state (θ=0) to the final state ($\theta=\pi$). In the case of the calculation, this energy barrier is 0.19 meV, which represents 2.2 K. On the contrary, the energy always decreases during the quasiuniform rotation. This proves once again that the system has found, on the energetic point of view, an easier reversal path for field induced magnetization reversal.

In zero field, there are two degenerate minima at θ=0 and π, separated by an energy barrier ΔE_0. It is very surprising to note that, although the two curves do not superimpose, and that, in the case of the quasiuniform reversal, the energy is lower or equal to the energy of the macrospin during reversal, the energy barrier is the same for the two reversal modes: $\Delta E_0 = N k_{\text{eff}}$. The reason is that, for the quasiuniform rotation, the worst energetic situation, at $\theta=\pi/2$, is perfectly monodomain. As a consequence, the macrospin model would perfectly describe the thermal magnetization reversal in zero (or small) field, like in finite temperature zero field susceptibility measurements.[14,21]

V. CONCLUSION

We have studied the limits of the macrospin model in Co nanodots, with an enhanced magnetocrystalline anisotropy at

the edge. An atomic description including every magnetic energy term (Zeeman energy, nearest neighbor exchange, magnetocrystalline anisotropy, and dipolar coupling) in the calculation has been used to find the equilibrium magnetic configurations and study the field induced magnetization reversal. The results have been compared with the macrospin model and a continuous micromagnetic model. We have shown that, for these dots, the macrospin model is oversimplified even for dots with diameter as low as 2 nm. Twisted magnetic configurations as well as the reduction of the magnetization switching field were observed in the simulation, indicating that the magnetic configurations are not always homogeneous at these small sizes. Significative reductions of the switching field have also been evidenced whereas only a small deviation to the coherent rotation of the magnetization was observed, a process that may be called quasiuniform rotation. Surprisingly, a good agreement was obtained with a continuous one dimensional micromagnetic model, the discrete character of the problem being only taken into account via a renormalization of the different parameters. This model gives a good description of the magnetic configuration and of the magnetization reversal of the nanodots.

Although the nanodots display a reduced switching field as compared to the case of the macrospin, they still have the same switching energy barrier in zero field. As a consequence, their thermal stability is the same as for macrospins, but they are easier to reverse with a magnetic field. This makes them interesting for information storage applications, where both high thermal stability and low reversal field are needed. In fact, their soft core and hard shell give them magnetic properties close to the exchange-spring magnets.[31,32]

ACKNOWLEDGMENT

We gratefully acknowledge O. Fruchart for stimulating discussions.

*rohart@lps.u-psud.fr

[1] A. Hubert and R. Schäfer, *Magnetic Domains* (Springer, Berlin, 1998).
[2] E. Stoner and E. Wohlfarth, Philos. Trans. R. Soc. London, Ser. A **240**, 599 (1948).
[3] W. F. Brown, Phys. Rev. **130**, 1677 (1963).
[4] J. Miltat, G. Albuquerque, and A. Thiaville, *Magnetism and Synchrotron Radiation* (Springer, Berlin, 2001), pp. 129–156.
[5] B. Barbara, *Magnetism and Synchrotron Radiation* (Springer, Berlin, 2001), pp. 156–208.
[6] *Surface Effects in Magnetic Nanoparticles*, edited by D. Fiorani (Springer, Berlin, 2001).
[7] W. T. Coffey, D. S. F. Crothers, J. L. Dormann, Y. P. Kalmykov, E. C. Kennedy, and W. Wernsdorfer, Phys. Rev. Lett. **80**, 5655 (1998).
[8] A. Thiaville, Phys. Rev. B **61**, 12221 (2000).
[9] M. Respaud, J. M. Broto, H. Rakoto, A. R. Fert, L. Thomas, B. Barbara, M. Verelst, E. Snoeck, P. Lecante, A. Mosset, J. Osuna, T. O. Ely, C. Amiens, and B. Chaudret, Phys. Rev. B **57**, 2925 (1998).
[10] E. Bonet, W. Wernsdorfer, B. Barbara, A. Benoît, D. Mailly, and A. Thiaville, Phys. Rev. Lett. **83**, 4188 (1999).
[11] M. Jamet, W. Wernsdorfer, C. Thirion, D. Mailly, V. Dupuis, P. Mélinon, and A. Pérez, Phys. Rev. Lett. **86**, 4676 (2001).
[12] S. I. Woods, J. R. Kirtley, S. Sun, and R. H. Koch, Phys. Rev. Lett. **87**, 137205 (2001).
[13] P. Allia, M. Coisson, P. Tiberto, F. Vinai, M. Knobel, M. A. Novak, and W. C. Nunes, Phys. Rev. B **64**, 144420 (2001).
[14] S. Rusponi, T. Cren, N. Weiss, M. Epple, P. Buluschek, L. Claude, and H. Brune, Nat. Mater. **2**, 546 (2003).
[15] E. Tronc, A. Ezzir, R. Cherkaoui, C. Chanéac, M. Noguès, H. Kachkachi, D. Fiorani, A. M. Testa, J. M. Grenèche, and J. P. Jolivet, J. Magn. Magn. Mater. **221**, 63 (2000).
[16] P. Gambardella, S. Rusponi, M. Veronese, S. Dhesi, C. Grazioli, A. Dallmeyer, I. Cabria, R. Zeller, P. Dederichs, K. Kern, C. Carbone, and H. Brune, Science **300**, 1130 (2003).
[17] D. A. Dimitrov and G. M. Wysin, Phys. Rev. B **50**, 3077 (1994).
[18] H. Kachkachi and M. Dimian, Phys. Rev. B **66**, 174419 (2002).
[19] D. A. Garanin and H. Kachkachi, Phys. Rev. Lett. **90**, 065504 (2003).
[20] J.-C. Levy, M. Krawczyk, and H. Puszkarski, J. Magn. Magn. Mater. **305**, 182 (2006).
[21] N. Weiss, T. Cren, M. Epple, S. Rusponi, G. Baudot, S. Rohart, A. Tejeda, V. Repain, S. Rousset, P. Ohresser, F. Scheurer, P. Bencok, and H. Brune, Phys. Rev. Lett. **95**, 157204 (2005).
[22] S. Rohart, V. Repain, A. Tejeda, P. Ohresser, F. Scheurer, P. Bencok, J. Ferré, and S. Rousset, Phys. Rev. B **73**, 165412 (2006).
[23] F. Meier, K. von Bergmann, P. Ferriani, J. Wiebe, M. Bode, K. Hashimoto, S. Heinze, and R. Wiesendanger, Phys. Rev. B **74**, 195411 (2006).
[24] R. Skomski and J. M. D. Coey, *Permanent Magnetism* (Institute of Physics, London, 1999).
[25] E. Y. Vedmedenko, H. P. Oepen, and J. Kirschner, J. Magn. Magn. Mater. **256**, 237 (2003).
[26] M. Beleggia, M. D. Graef, Y. Millev, D. Goode, and G. Rowlands, J. Phys. D **38**, 3333 (2005).
[27] A. Thiaville and A. Fert, J. Magn. Magn. Mater. **113**, 161 (1992).
[28] A. Rettori, L. Trallori, P. Politi, M. Pini, and M. Macció, J. Magn. Magn. Mater. **140-144**, 639 (1995).
[29] A. Thiaville, J. Magn. Magn. Mater. **182**, 5 (1998).
[30] H. Kachkachi and E. Bonet, Phys. Rev. B **73**, 224402 (2006).
[31] R. Skomski and J. M. D. Coey, Phys. Rev. B **48**, 15812 (1993).
[32] H. Zeng, J. Li, J. Liu, Z. Wang, and S. Sun, Nature (London) **420**, 395 (2002).